Structure determination of the zeolite IM-5 using electron crystallography

Junliang Sun[I, II] Zhanbing He[I], Sven Hovmöller[I], Xiaodong Zou[*, I, II], Fabian Gramm[III, IV], Christian Baerlocher[III] and Lynne B. McCusker[III]

[I] Inorganic and Structural Chemistry, Department of Materials and Environmental Chemistry Stockholm University, 106 91 Stockholm, Sweden
[II] Berzelii Centre EXSELENT on Porous Materials, Stockholm University, 106 91 Stockholm, Sweden
[III] Laboratory of Crystallography, ETH Zurich, 8093 Zurich, Switzerland
[IV] Electron Microscopy ETH Zurich (EMEZ), 8093 Zurich, Switzerland

Abstract. The structure of the complex zeolite IM-5 (*Cmcm*, $a = 14.33(4)$ Å, $b = 56.9(2)$ Å, $c = 20.32(7)$ Å) was determined by combining selected area electron diffraction (SAED), 3D reconstruction of high resolution transmission electron microscopy (HRTEM) images from different zone axes and distance least squares (DLS) refinement. The unit cell parameters were determined from SAED. The space group was determined from extinctions in the SAED patterns and projection symmetries of HRTEM images. Using the structure factor amplitudes and phases of 144 independent reflections obtained from HRTEM images along the [100], [010] and [001] directions, a 3D electrostatic potential map was calculated by inverse Fourier transformation. From this 3D potential map, all 24 unique Si positions could be determined. Oxygen atoms were added between each Si−Si pair and further refined together with the Si positions by distance-least-squares. The final structure model deviates on average 0.16 Å for Si and 0.31 Å for O from the structure refined using X-ray powder diffraction data. This method is general and offers a new possibility for determining the structures of zeolites and other materials with complex structures.

1. Introduction

Zeolites have attracted considerable interest because of their diverse industrial applications in the areas of catalysis, separation and ion exchange. In particular, the synthesis of new high-silica zeolites has been actively pursued, because these zeolites tend to have higher thermal stability and consequently wider applications [1]. Structural information is fundamental to the understanding of zeolite chemistry and therefore to its application and possible modification. Unfortunately, most high-silica zeolites are polycrystalline or not even pure phases, and this has made the determination of their structures extremely difficult.

X-ray powder diffraction has been one of the most important techniques for solving the structures of unknown zeolites [2]. Several novel approaches such as incorporating crystal chemical information (FOCUS) [3, 4], using pore/channel information to generate structure envelopes [5, 6], or using textured samples to generate more single-crystal-like data [7, 8] have been developed for this purpose. However, when the structures become too complex and a large portion of the reflections overlap in the powder diffraction pattern, structure determination from X-ray powder diffraction data alone is very difficult.

Recently X-ray powder diffraction has been combined with electron crystallography to determine the structures of several complex zeolites: TNU-9 [9], IM-5 [10], SSZ-74 [11] and ITQ-37 [12]. The advantages of electron crystallography as a complementary tool to powder diffraction are twofold: (1) electrons interact much more strongly with atoms than do X-rays, so polycrystalline materials down to 10 nm behave like single crystals with electrons on a TEM, and (2) the crystallographic structure factor phases, which are lost in a diffraction experiment, can be obtained from high resolution transmission electron microscopy (HRTEM) images. The phase information facilitates structure solution significantly.

Electron crystallography has been used to determine the structures of a large range of polycrystalline compounds, especially nano- and micro-sized crystallites. These include minerals [13], oxides [14–17], metal clusters [18–20], and intermetallic compounds [21]. One complex structure of *v*-AlCrFe with $a = 40.687$ Å, $c = 12.546$ Å, space group $P6_3/m$ was solved by combining information from HRTEM images and selected area electron diffraction (SAED) patterns from 13 zone axes [21]. There, 124 of the 129 unique atoms were determined by electron crystallography. Even structures of membrane proteins have been solved by electron crystallography [22, 23]. Thus, it is clear that extremely complex structures can be solved by electron crystallography. Electron crystallography has also been applied to zeolites and ordered mesoporous materials [24–29]. The

* Correspondence author (e-mail: xiaodong.zou@mmk.su.se)

structures of many interesting zeolites and related porous materials remain unsolved, because the samples contain more than one phase, have defects and/or the structures are just too complex to be solved from X-ray powder diffraction data alone. In such cases, the advantages of electron crystallography come to light.

Recently a novel approach to structure solution using a charge-flipping algorithm was reported [30]. Several complex zeolite structures have been solved by combining X-ray powder diffraction data and electron crystallography using this new approach [10–12]. One example is that of the high-silica zeolite catalyst IM-5, whose synthesis was first reported in 1998 [31]. It has proven to be an important thermally stable catalyst for hydrocarbon cracking and NO reduction [32]. IM-5 is one of the most complex known zeolites, with 24 Si-atoms in the asymmetric unit, and crystallizes only in polycrystalline form. Even the unit cell dimensions are difficult to determine from X-ray powder diffraction data, because the large unit cell and coincidental relationships between the lengths of the axes cause an extreme degree of reflection overlap. Electron diffraction, however, is a single crystal technique and all reflections are recorded individually. This makes electron diffraction very powerful for the determination of unit cell parameters. Originally, the structure of IM-5 could only be solved by combining transmission electron microscopy and X-ray powder diffraction data in a charge-flipping structure solution algorithm [10].

It is important to know if the structures of materials as complex as IM-5 can be solved by electron crystallography. It is also important to establish a general approach for doing so. In this paper, we examine a complete *ab initio* structure determination of the zeolite IM-5 using only electron crystallography and no prior structure information.

2. Experiments

The sample of IM-5 was synthesized by Benazzi et al. as reported earlier [31]. A small amount of IM-5 sample was ground to a fine powder and dispersed in acetone. A drop of this suspension was transferred onto a holey carbon film supported by a copper grid. SAED patterns were collected on Philips CM-30, JEOL JEM-3010 and JEOL JEM-2000FX transmission electron microscopes operated at 300 kV, 300 kV and 200 kV, respectively. For the determination of the unit cell parameters, several tilt series of SAED patterns were collected by tilting the crystals around diffraction rows with the shortest reciprocal distances. HRTEM images were obtained along the main axes on JEOL JEM-3010 transmission electron microscopes at 300 kV (point resolution 1.7 Å). The SAED patterns and HRTEM images were recorded by a Gatan multiscan A40 or Keenview CCD cameras. To minimize the dynamic effects, only the thinnest edges of the crystals were selected for SAED and HRTEM.

All SAED patterns were analyzed by the program ELD [33]. The program Trice [34] was used to combine the SAED patterns from each tilt series, with the positions and intensities given by ELD, into 3D reciprocal space.

The unit cell parameters were then determined from the 3D reciprocal space. Crystallographic image processing of the HRTEM images was performed by the program CRISP [35]. For each HRTEM image, the thinnest part of the crystal was selected and its Fourier transform was calculated. The corresponding contrast transfer function (CTF) was estimated from the Fourier transform, and the effects of the CTF were compensated for. The positions of the diffraction spots were determined and the corresponding reciprocal lattice was refined. The amplitude and phase were then extracted from each diffraction spot. Note that due to the lath-like crystal morphology of IM-5 (Fig. 1), crystals were mostly oriented with the *a*-axis perpendicular to the holey carbon film. While HRTEM images with large thin areas (>100 nm) were relatively easy to obtain in the [100] projection, it was very difficult to find the [010] and [001] directions under TEM, especially crystals containing thin areas in the projections. In the best cases, very small thin areas (10–20 nm) could be obtained at the edges of the crystals in [010] and [001] projections. They were just enough for the image processing.

In order to determine the projection symmetry of the crystal, all possible plane groups were tested to see which one best fitted the experimental image. The corresponding projection symmetry was determined only from the phases, since different plane groups can give the same amplitude relationships. In addition, a slight crystal misalignment can introduce large changes in the amplitudes, but not in the phases. For each plane group, the phases of symmetry-related reflections obey some simple relationships if the origin is at a symmetry element. For example, a 2-fold axis is always selected as the origin for the plane group *p*2, and then all phases are restricted to 0 or 180°. A weighted average difference between the experimental phases and the phases after imposing the phase relations and restrictions is defined as the phase residual (φ_{res}). It is calculated using the equation:

$$\varphi_{\text{res}} = \sum_{hk} A_{hk} \, \Delta\varphi_{hk} \bigg/ \sum_{hk} A_{hk}$$

where A_{hk} is the amplitude of reflection *hk* and Δf_{hk} is the phase error of reflection *hk*. When the origin is moved to a different position within a unit cell, all phases will be changed accordingly, while amplitudes remain the same. So, for a certain plane group, by searching throughout the whole unit cell, we can find the origin(s) that correspond to the lowest phase residual φ_{res}. The origin is then moved to such an origin. The R-value for symmetry-related reflections and the lowest phase residual were calculated for each possible plane group. The plane group that corresponds to the lowest phase residual φ_{res} and highest possible symmetry will be chosen as the correct projection symmetry.

Finally, the projection symmetry was applied to the amplitudes and phases. The amplitudes for the symmetry-related reflections are set to be equal. The phases of all reflections were adjusted to correspond to the nearest possible phases according to the phase relationships and the phase restrictions. For example, for projections containing a 2-fold axis, all phases were adjusted to the nearest of 0° or 180°. The final amplitudes and phases will be

close to those of the structure factors, if the crystal is thin enough. A projection of the potential map can be calculated by inverse Fourier transform using the amplitudes and phases after imposing the projection symmetry. The reflections obtained from HRTEM images along different zone axes were merged together. A 3D electrostatic potential map was calculated using the program eMap [36], and the atomic positions were determined from this 3D potential map. The geometry of the final structure model was optimized using the distance least-squares program DLS-76 [37]. SAED patterns were simulated using the program MacTempas [38], and the atomic coordinates from the model.

3. Results and discussion

The complete structure determination of IM-5 is divided into the following steps: (1) determination of the unit cell, lattice type and Laue group from SAED patterns, (2) determination of the projection symmetry and crystal structure factors from each HRTEM image, (3) 3D reconstruction from different projections and determination of atomic positions, (4) structure optimization by distance least-squares refinement, and (5) structure verification. Each step is described in detail below.

3.1 Determination of unit cell, lattice type and Laue group

A general way of determining the unit cell is from a tilt series of SAED patterns, as shown in Fig. 1. The 2D lattice for each SAED pattern was detected and further refined using the program ELD [33]. The positions, d-values and intensities of all diffraction spots were extracted. This information, together with the corresponding tilt angle for each SAED pattern in the tilt series, was used to reconstruct the 3D reciprocal space using the program Trice [34]. From the reconstructed 3D reciprocal lattice, the cell parameters were determined to be $a = 14.1(5)$ Å, $b = 56.9(1)$ Å, $c = 19.8(1)$ Å, $\alpha = 90.0(3)°$, $\beta = 90.8(6)°$, $\gamma = 89.6(5)°$. The reflection condi-

tion was $h + k = 2n$ for all reflections, indicating that IM-5 is C-centered.

To check whether IM-5 is orthorhombic or adopts a lower symmetry, its Laue class needs to be determined. The SAED pattern along the [100] direction clearly shows 2mm symmetry (see Fig. 1). All SAED patterns obtained by tilting the crystal around the b^*-axis show a mirror-symmetry perpendicular to the b^*-axis. Thus, the crystal has a mirror symmetry perpendicular to the b^* axis in reciprocal space. Similarly, the crystal has a mirror symmetry perpendicular to the c^*-axis in reciprocal space. Since reciprocal space is always centrosymmetric, there must also be a mirror symmetry perpendicular to the a^*-axis. Thus, the diffraction pattern of IM-5 belongs to the Laue class mmm and its unit cell is C-centred orthorhombic. The similar intensity distributions and tilt angles of the symmetry-related SAED patterns (for example [501] and [−5 0 1], [301] and [−3 0 1] and [11 1 0] and [−11 1 0] in Fig. 1) further confirm the mirror symmetry perpendicular to the a^*-axis. The deviations of unit cell angles from 90° were caused by lens distortions of the TEM instrument [39], errors of the tilt angles due to the goniometer, and sample misalignment. The final unit cell parameters were obtained from the SAED patterns taken along the three main zone axes (see Fig. 2a–c) as $a = 14.1$ Å, $b = 57.0$ Å and $c = 19.8$ Å, because these are usually more accurate than those obtained from a tilt series.

3.2 Determination of space group

The space group of IM-5 can be deduced from the systematic absences observed in the SAED patterns taken along the three main zone axes (shown in Fig. 2a–c). This gives the following reflection conditions: hkl: $h + k = 2n$; $0kl$: $k = 2n$; $h0l$: $h = 2n$, $l = 2n$; $hk0$: $h + k = 2n$; $h00$: $h = 2n$; $0k0$: $k = 2n$; $00l$: $l = 2n$.

There are only 3 possible space groups corresponding to these reflection conditions: $Cmc2_1$, $C2cm$ and $Cmcm$ [11]. These three space groups have the same systematic absences and can not be distinguished from diffraction

Fig. 1. A series of SAED patterns from the same crystal of IM-5 tilted along the two shortest perpendicular reciprocal axes. The tilt axes are indicated by arrows. The corresponding tilt angle for each SAED pattern is given. The unit cell parameters were determined from the tilt series and the SAED patterns were then indexed. SAED patterns along the [501], [−5 0 1], [301] and [−3 0 1] directions show a mirror-symmetry perpendicular to the b^*-axis. Thus, the crystal has a mirror symmetry perpendicular to the b^* axis in reciprocal space. Similarly, the SAED patterns along the [100], [11 1 0] and [−11 1 0] directions all have the mirror-symmetry perpendicular to the c^*-axis. A TEM image of a typical plate-like IM-5 crystal is inserted.
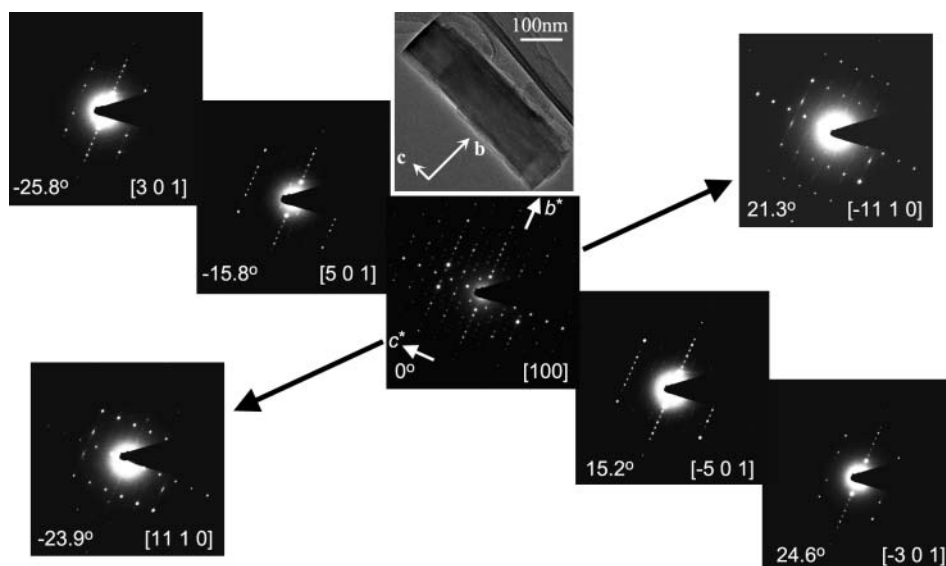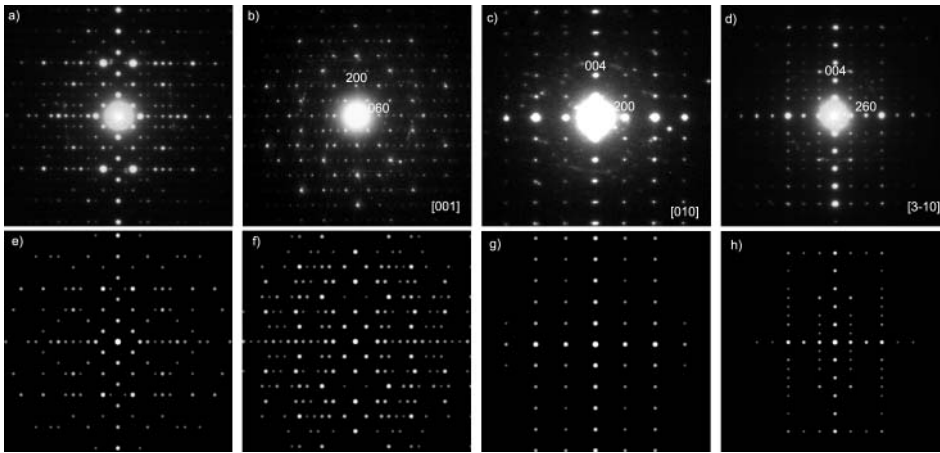
Fig. 2. Experimental SAED patterns of IM-5 taken along (**a**) [100], (**b**) [001], (**c**) [010] and (**d**) [3 −1 0] directions. The corresponding simulated ED patterns along (**e**) [100] (thickness $t = 100$ Å), (**f**) [001] ($t = 180$ Å), (**g**) [010] ($t = 200$ Å) and (**h**) [3 −1 0] ($t = 150$ Å) directions. The accelerating voltage was 300 kV.

data. However, their projection symmetries are different, as shown in Table 1. Since HRTEM images maintain the phase information, it is possible to determine the projection symmetries from HRTEM images. In this way, we can uniquely determine the space group.

HRTEM images along the three main zone axes are shown in Fig. 3. The projection symmetry was determined by crystallographic image processing using the program CRISP [35] (Fig. 4). Amplitudes and phases for all observed reflections were extracted from the Fourier transform of each HRTEM image. The corresponding lowest phase residual φ_{res} was given for each plane group. The lowest phase residuals for the HRTEM image along the [100] projection are 4.5°, 9.1° and 11.1°, corresponding to *pm* ($m \perp c$), *pg* ($g \perp b$) and *pmg* ($m \perp c$) symmetries, respectively (Table 2). Since *pmg* is a supergroup of *pm* and *pg* and its phase residue is only higher by a few degrees than those for *pm* and *pg*, the higher projection symmetry *pmg* is the most reasonable one for IM-5 along the [100] direction. The projection symmetries along the [010] and [001] directions were obtained in a similar way from the HRTEM images, and found to be *pmm* and *cmm*, respectively, by comparing the corresponding phase residuals (see Table 2). The space group of IM-5 could be then deduced from the projection symmetries from the three main directions, to be *Cmcm*, according to Table 1.

The phase residuals φ_{res} along the three main zone axes are 11.1, 13.2 and 16.0°, corresponding to the symmetries *pm*g, *pmm* and *cmm*, respectively. As a rule of thumb, phase residuals less than 20° are often acceptable so that the space group *Cmcm* is the most probable one. It is worth mentioning that due to the lath-like shape of the IM-5 crystals (see Fig. 1), the crystals along [010] and [001] directions are relatively thick, which makes the symmetry determination less reliable for those projections. We cannot completely rule out the possibility that the real structure may be slightly distorted from *Cmcm* symmetry.

For example, the projection symmetries along the [010] and [001] directions may be *pm* ($m \perp c$) and *cm* ($m \perp b$), which gave much lower phase residuals (3.7 and 6.4°, respectively). In such a case, the space group would be *C2cm*.
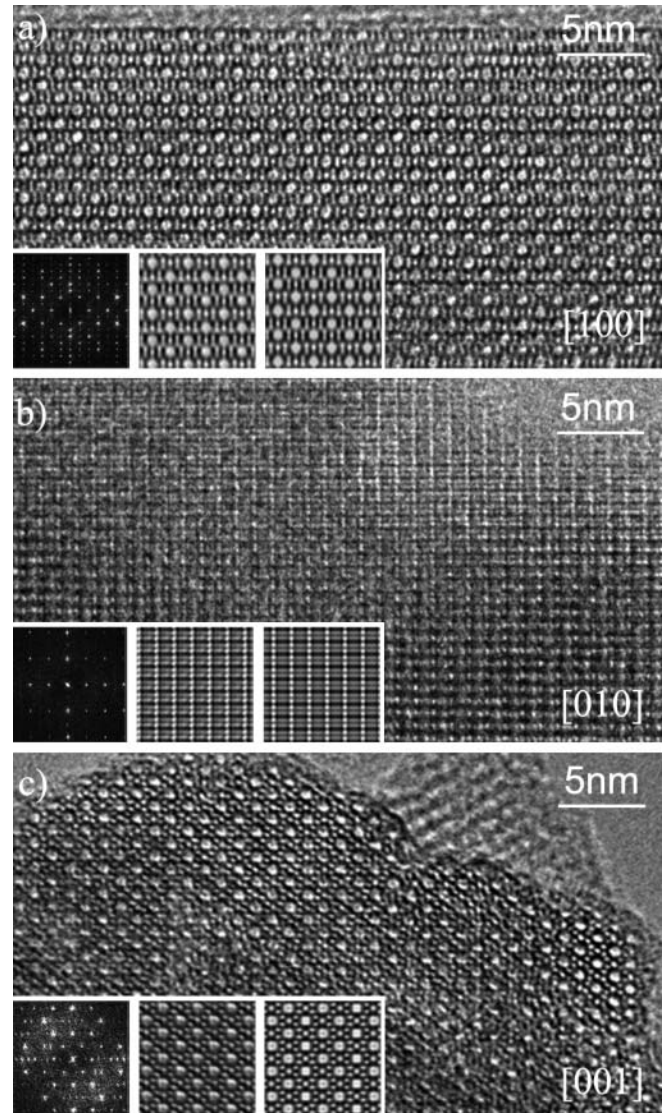
Fig. 3. HRTEM images along the three main crystallographic axes. The inserts show their corresponding Fourier transforms, lattice averaged images and images after imposing the *Cmcm* symmetry.

Table 1. Projection symmetries for three possible space groups.

Space group	[100]	[010]	[001]
$Cmc2_1$	pg	pm ($m \perp a$)	cmm
C2cm	pmg	pm ($m \perp c$)	cm ($m \perp b$)
Cmcm	pmg	pmm	cmm

Fig. 4. Determination of projection symmetry and retrieval of the structure projection from an HRTEM image taken along the [100] direction by crystallographic image processing using CRISP [39]. The lowest phase residuals are 4.5°, 9.1° and 11.1°, corresponding to *pm* (*m* ⊥ *c*), *pg* (*g* ⊥ *b*) and *pmg* (*m* ⊥ *c*) symmetries, respectively. Since *pmg* is a supergroup of *pm* and *pg* and its phase residue is only higher by a few degrees than those for *pm* and *pg*, the higher projection symmetry *pmg* is the most reasonable one. The final projected potential map after imposing the projection symmetry *pmg* is shown in the lower right.
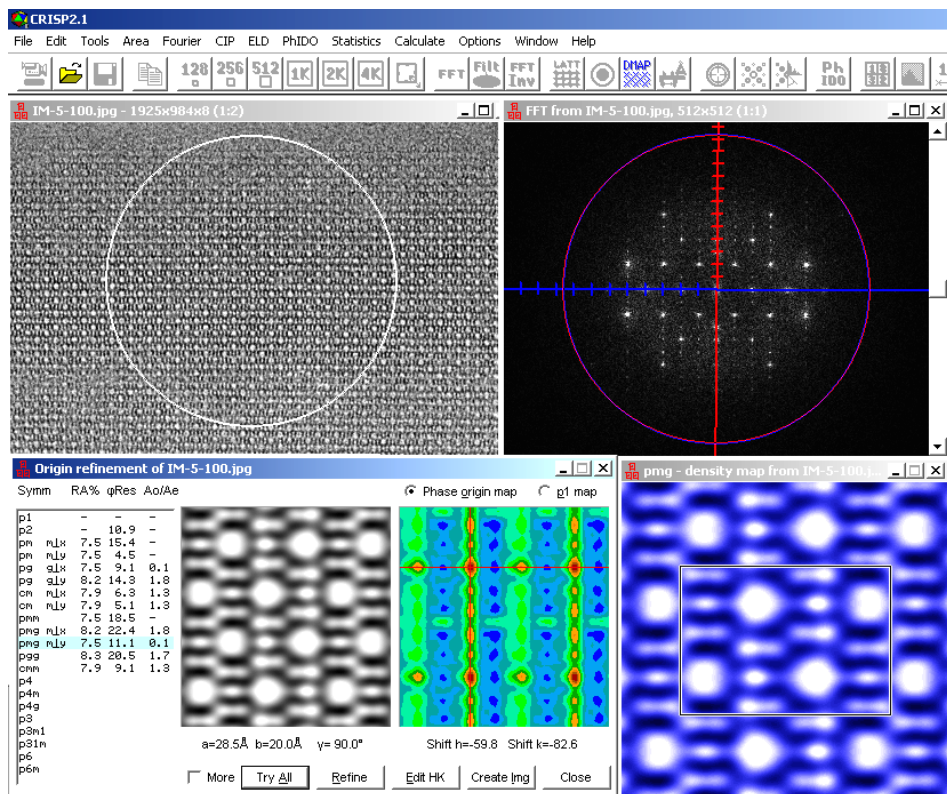
3.3 Reconstruction of projected potential maps and 3D potential map

Once the projection symmetry is determined, a 2D map can be calculated from the amplitudes and phases extracted from the HRTEM image by an inverse Fourier transform. After imposing the symmetry, the maps correspond to the projected potential (Fig. 5). 10-ring channels could be observed in the [100] and [001] projections, but not along the [010] direction. In addition, 4-, 5- and 6-rings can be identified in the [001] projection. Since atoms are overlapped in all projections, it is necessary to combine the HRTEM images from different projections to obtain a 3D potential map, from which the 3D atomic coordinates can be determined. The best approach is from reciprocal space, by merging the structure factor amplitudes and phases deduced from the Fourier transforms of the HRTEM images along the different projections.

A total of 281 reflections were obtained from the three projections (133 from [100], 34 from [010] and 114 from [001], Table S1 in the Supporting information), and of these, 144 were unique. Reflections from the [010] and [001] projections were merged into the reflection data from the [100] projection based on the common reflections, since the HRTEM image along the [100] direction

was the best one, with the thinnest area, the smallest phase residual φ_{res} and the highest resolution. One important step for merging the reflections is to select the same phase origin for the three projections. For each projection, there are four possible choices of origin. The common origin for the three projections is found when reflections to the different projections, especially the strongest ones, common have the same phases. The common reflections are 0*k*0 for the [100] and [001], 00*l* for the [100] and [010] and *h*00 for the [010] and [001] projections. In total, 14 pairs of common reflections were obtained, and 12 of them have consistent phases. The phase coherence of the common reflections shows the reliability of phases obtained from HRTEM images, which is essential for obtaining a correct potential map. The remaining two pairs of common reflections, (008) and (600), did not have the same phases for different projections. In both cases, the amplitudes of the reflection pair differed very much, 1454 and 164 for (008), and 750 and 203 for (600). This is due to dynamical effects. Here the amplitude and the phase of the strongest reflection from each pair were used for the 3D reflection data.

Once the common origin is found, new phases are recalculated according to the common origin by $\varphi_{new}(hkl) = \varphi_{old}(hkl) + 360 \, (hx_s + ky_s + lz_s)$, where

Table 2. Phase residuals corresponding to different projection symmetries.

Plane group	*pm* (*m* ⊥ *a*)	*pm* (*m* ⊥ *c*)	*pg* (*g* ⊥ *b*)	*cm* (*m* ⊥ *a*)	*cm* (*m* ⊥ *b*)	*pmg* (*m* ⊥ *c*)	*pmm*	*cmm*
[100]	–	4.5	9.1	–	–	11.1	–	–
[010]	9.3	3.7	–	–	–	–	13.2	–
[001]	–	–	–	7.8	6.4	–	–	16.0
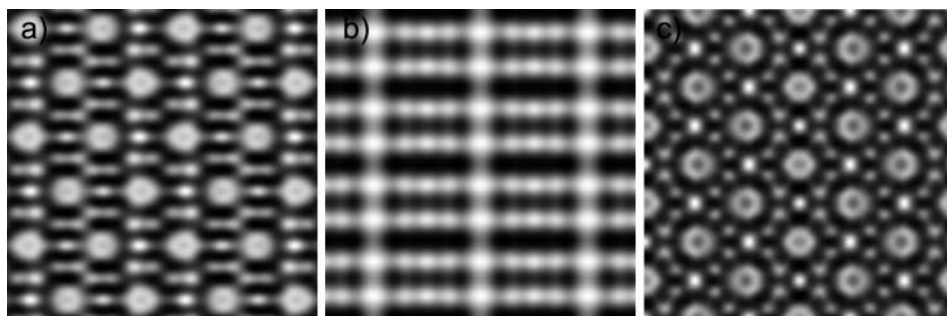
$(x_s y_s z_s)$ is the origin shift. Since the HRTEM images were taken near the Scherzer defocus where all reflections were inside the first zero-crossover of the contract transfer function, black features (low intensity) in the HRTEM images correspond to atoms while white features (high intensity) to pores. Consequently, all phases should be shifted by 180° to make them comparable to crystal structure factor phases. Then atom positions will correspond to high density, as is the case in density maps calculated in X-ray crystallography.

The amplitudes of the reflections from different projections were scaled to one another using the common reflections with the same phases. This resulted in 144 unique reflections and R_{int} was about 0.30 for *Cmcm* symmetry, which is acceptable for electron microscopy data. Some strong reflections, for example (0 0 10) extend to 2.0 Å resolution, which is sufficient for determining Si positions (a typical Si−Si distance is 3.1 Å).

Once the structure factor amplitudes and phases had been prepared, the 3D potential map of IM-5 was reconstructed by inverse Fourier transform using eMap (Fig. 6). With a proper threshold, a clear framework envelope was obtained. Since very few strong reflections were measured

beyond the resolution of a Si−Si distance (about 3.1 Å), the peaks in the 3D potential map are not well resolved. Nonetheless, 24 unique peaks could be identified inside the envelope and assigned to Si positions by changing the threshold to a higher value (Fig. 6). All of these Si positions are four-connected to others and are shown in Fig. 6a with an oxygen inserted between each Si−Si pair. The atomic coordinates for these 24 Si positions were determined from the 3D map and are listed in the Supporting Information.

3.4 Distance least squares refinement

Because of the relatively low resolution of the HRTEM images, the Si positions obtained from the 3D potential map were not accurate. In order to get more accurate positions, it is necessary to refine the Si positions either by performing a Rietveld refinement using powder diffraction data or by optimizing the geometry using a distance least squares (DLS) refinement if the sample is not pure or powder diffraction data are not available. Here, we choose the distance least squares refinement, using the program DLS-76 [37].

Before refinement, it is necessary to find the connections between all Si atoms. In some cases, not all connections were obvious. There are several rules for high-silica zeolites: all Si atoms are connected to four other Si atoms via oxygen atoms; 5- and 6-rings are more common than 3-rings or double 4-rings. For IM-5, most framework oxygen atoms are inside the envelope in Fig. 6a, and the connections through these oxygen atoms were obvious. The few remaining connections could be found easily using the rules above. In total, 47 independent Si−Si connections were found and the distances between the Si pairs varied from 2.3 to 4.2 Å.

Oxygen atoms were introduced exactly half-way between the 47 Si−Si pairs, and then 47 Si−Si (3.0824 Å), 94 Si−O (1.616 Å) and 120 O−O (2.639 Å) distances were specified and assigned the weights 1, 4, and 2, respectively. With these 261 distances, the 174 coordinates defining the 24 Si and 47 O atoms could be refined. After distance least-squares refinement, the structural model was significantly improved. Then, the unit cell parameters were refined together with all coordinates and became $a = 14.33(4)$ Å, $b = 56.9(2)$ Å and $c = 20.32(7)$ Å. All atomic coordinates are listed in the Supporting Information.

Fig. 6. A 3D potential map reconstructed from 144 unique reflections using the program eMap [36]. (**a**) An overview of the 3D potential map (cyan is towards the wall and blue towards the pores) with the structure model derived from it, and (**b**) a 2D projection of the 3D potential map along the *c*-axis. (**c**) The Si framework viewed along the *c*-axis in the final structural model.
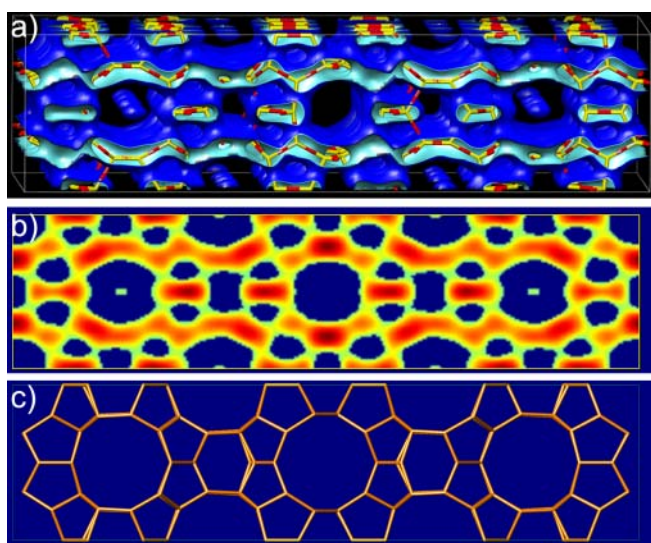
In this final structural model, the estimated standard deviations of the atomic positions are about 0.1 Å for Si and 0.2 Å for O atoms, and this is sufficiently accurate to allow further refinement with X-ray diffraction data. All bond distances and most angles are reasonable. The only exception is Si10−O25−Si10, which is constrained to be 180° by the *Cmcm* symmetry (see Supporting Information). Compared with the initial positions obtained from the 3D potential map, the largest shift of Si positions is 0.88 Å (for Si4) which might be due to the incompleteness and low accuracy of the data. Nonetheless, all final Si positions are in the high density region shown in Fig. 6a, and this means that even if some of the Si atoms moved considerably, the final structure model is still consistent with the potential map.

3.5 Structure verification

The procedure described above allowed all the atomic positions for Si and O for IM-5 to be obtained. The question is how reliable the final structure model is. Since the structure is already known [10], our final structural model can be compared directly with the published one to get some feeling about its reliability. The unit cell parameters obtained from the SAED patterns were close to the reported ones with a deviation about 1%.

The phases the strongest 53 reflections obtained by electron crystallography are the same as those calculated from the published structure, with the exception of three relatively weak ones, (5 9 0, 8 0 0) and 3 21 0. The amplitudes of these three reflections are approximately 4−5% of the strongest reflection. All amplitudes with incorrect phases in all 144 reflections add up to only 7.5% of the total amplitude sum, which will only give very minor contributions to the final 3D potential map.

The amplitudes are also close to the calculated ones. Some peaks with low *d*-values (*e.g.* 0 0 10, 008, etc.) have much weaker intensities than they should, because no correction was made for the curvature of the Ewald sphere. This was not done because the thickness of the crystal was not known. The deviation of the amplitudes is about 37% for the 53 strongest reflections. In summary, both phases and amplitudes were consistent with those calculated from the published structure with acceptable deviations, and sufficiently small to allow the correct structural model to be found.

The 24 Si atomic positions obtained from HRTEM images are quite close to the ones refined by X-ray powder diffraction, with an average deviation of 0.47 Å. After DLS refinement, the average deviations decreased to 0.16 Å for Si and 0.31 Å for O, and the largest deviations were 0.35 Å for Si5 and 0.89 Å for O13. As shown in Fig. 7, our final structure model and the structure refined by X-ray powder diffraction match very well.

If IM-5 had been a totally unknown structure, the quality of the structural model would have to be checked differently. Of course, the reliability of each step described above would have to be examined carefully, but the observed SAED patterns could also be compared with those calculated from the structural model. Four calculated SAED patterns are shown in Fig. 2e−h and they show

[100]

[001]
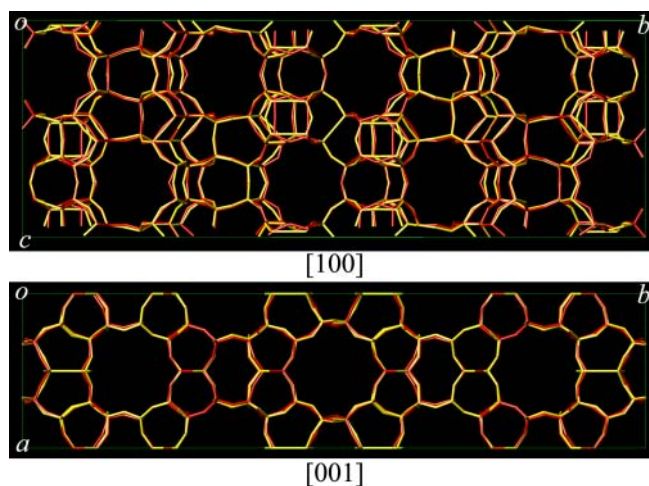
Fig. 7. Final structure model (in yellow) compared with the structure refined by X-ray powder diffraction (in red). The average deviations are 0.16 Å for Si atoms and 0.31 Å for oxygen. The largest deviations are 0.89 Å for O13 and 0.35 Å for Si5.

good agreements with the experimental SAED patterns (Fig. 2a−d). So, even without knowing the structure, we could assess the model obtained from HRTEM images. For all the simulated SAED patterns in Fig. 2, large thicknesses were used (100 ∼ 200 Å), and the dynamic effects are significant. This is why we used the amplitudes from the HRTEM images rather than those from SAED patterns for the 3D reconstruction.

The SAED patterns can be interpreted further in view of the final model. The IM-5 structure is dominated by 5- and 10-rings along the [001] direction (Fig. 6). The strong reflections along the [001] direction show a *pseudo* 10-fold symmetry at the resolution about 3.5 Å (Fig. 2b). It can also be observed that every third reflection along the b^*-axis in Fig. 2b is strong, indicating that the structure has a *pseudo* three-fold super-lattice as shown in Fig. 6c. Turning to the [100] direction, there are 4 large pores per unit cell along the *b* axis, and the corresponding SAED pattern shows that every fourth reflection along the b^*-axis is strong. Thus the final model is in good agreement with the experimental SAED patterns.

4. Conclusions

The unit cell and space group of the complex zeolite IM-5 were obtained directly from SAED patterns and HRTEM images. A structural model of IM-5 was deduced by electron crystallography from HRTEM images along the three main zone axes and then refined by DLS. The final structural model is very close to the structure refined by X-ray powder diffraction, with atomic positions differing on average by 0.16 Å for Si and 0.31 Å for O. The method presented here is especially useful for crystals that are too small, samples that are not pure, or zeolites with complicated structures.

References

[1] Corma, A.: Inorganic Solid Acids and Their Use in Acid-Catalyzed Hydrocarbon Reactions. Chem. Rev. **95** (1995) 559–614.

[2] Wessels, T.; Baerlocher, Ch.; McCusker, L.B.; Creyghton, E.J.: An ordered form of the extra-large-pore zeolite UTD-1: synthesis and structure analysis from powder diffraction data. J. Am. Chem. Soc. **121** (1999) 6242–6247.

[3] Grosse-Kunstleve, R.W.; McCusker, L.B.; Baerlocher, Ch.: Zeolite structure determination from powder diffraction data: applications of the FOCUS method. J. Appl. Cryst. **32** (1999) 536–542.

[4] Grosse-Kunstleve, R.W.; McCusker, L.B.; Baerlocher, Ch.: Powder Diffraction Data and Crystal Chemical Information Combined in an Automated Structure Determination Procedure for Zeolites. J. Appl. Cryst. **30** (1997) 985–995.

[5] Brenner, S.; McCusker, L.B.; Baerlocher, Ch.: The application of structure envelopes in structure determination from powder diffraction data. J. Appl. Cryst. **35** (2002) 243–252.

[6] Brenner, S.; McCusker, L.B.; Baerlocher, Ch.: Using a structure envelope to facilitate structure solution from powder diffraction data. J. Appl. Cryst. **30** (1997) 1167.

[7] Wessels, T.; Baerlocher, Ch.; McCusker, L.B.: Single-crystal-like diffraction data from polycrystalline materials. Science **284** (1999) 477–479.

[8] Baerlocher, Ch.; McCusker, L.B.; Prokic, S.; Wessels, T.: Exploiting texture to estimate the relative intensities of overlapping reflections. Z. Kristallogr. **219** (2004) 803–812.

[9] Gramm, F.; Baerlocher, Ch.; McCusker, L.B.; Warrender, S.J.; Wright, P.A.; Han, B.; Hong, S.B.; Liu, Z.; Ohsuna T.; and Terasaki, O.: Complex zeolite structure solved by combining powder diffraction and electron microscopy. Nature **444** (2006) 79–81.

[10] Baerlocher, Ch.; Gramm, F.; Massüger, L.; McCusker, L. B.; He, Z. B.; Hovmöller, S.; Zou, X. D.: Structure of the polycrystalline zeolite catalyst IM-5 solved by enhanced charge flipping. Science **315** (2007) 1113–1116.

[11] Baerlocher, Ch.; Xie, D.; McCusker, L.B.; Hwang, S.J.; Chan, I.Y.; Ong, K.; Burton, A.W.; Zones, S.I.: Ordered silicon vacancies in the framework structure of the zeolite catalyst SSZ-74. Nature Mater. **7** (2008) 631–635.

[12] Sun, J.L.; Bonneau, C.; Cantín, Á.; Corma, A.; Díaz-Cabañas, M.J.; Moliner, M.; Zhang, D.L.; Li, M.R.; Zou, X.D.: The ITQ-37 mesoporous chiral zeolite. Nature 458 (2009) 1154–1157.

[13] Downing, K.H.; Meisheng, H.; Wenk, H.R.; O'Keefe, M.A.: Resolution of oxygen atoms in staurolite by three-dimensional transmission electron microscopy. Nature **348** (1990) 525–528.

[14] Hovmöller, S.; Sjögren, A.; farrants, G.; Sundberg, M.; Marinder, B.O.: Accurate Atomic Positions from Electron Microscopy. Nature **311** (1984) 238–241.

[15] Wang, D. N.; Hovmöller, S.; Kihlborg, L.; Sundberg, M.: Structure Determination and Correction for Distortions in HREM by Crystallographic Image Processing. Ultramicroscopy **25** (1988) 303–316.

[16] Wang, Y.M.; Wang, H.B.; Li, F.H.; Jia, L.S.; Chen, X.L. Maximum entropy image deconvolution applied to structure determination for crystal $Nd_{1.82}Ce_{0.15}CuO_{4-d}$. Micron **36** (2005) 393–400.

[17] Bougerol-Chaillout, C.: Structure determination of oxide compounds by electron crystallography. Micron **32** (2001) 473–479.

[18] Weirich, T. E.; Ramlau, R.; Simon, A.; Hovmöller, S.; Zou, X. D.: A crystal structure determined to 0.02 Å accuracy by electron microscopy. Nature **382** (1996) 144–146.

[19] Zandbergen, H. W.; Andersen, S. J.; Jansen, J.: Structure Determination of Mg_5Si_6 Particles in Al by Dynamic Electron Diffraction Studies. Science **277** (1997) 1221–1225.

[20] Weirich, T. E.: Electron crystallography without limits? Crystal structure of $Ti_{45}Se_{16}$ redetermined by electron diffraction structure analysis. Acta Cryst. **A57** (2001) 183–191.

[21] Zou, X. D., Mo, Z. M., Hovmöller, S., Li, X. Z., Kuo, K. H.: Three-dimensional reconstruction of the *v*-AlCrFe phase by electron crystallography. Acta Crystallogr. **A59** (2003) 526–539.

[22] Henderson, R.; Unwin, P.N.T.: Three-dimensional model of purple membrane obtained by electron microscopy. Nature **257** (1975) 28–32.

[23] Bullough, P.A.; Henderson, R.: Phase accuracy in high-resolution electron microscopy of trigonal and orthorhombic purple membrane. Biophys. J. **58** (1990) 705–711.

[24] Nicolopoulos, S.; Conzález-Calbet, J.M.; Vallet-Regí, M.; Corma, A.; Corell, C.; Guil, J.M.; Pérez-Pariente, J.: Direct Phasing in Electron Crystallography: Ab initio determination of a new MCM-22 zeolite structure. J. Am. Chem. Soc. **117**, (1995) 8947–8956.

[25] a) Wagner, P.; Terasaki, O.; Ritsch, S.; Nery, J. G.; Zones, S. I.; Davis, M. E.; Hiraga, K.: Electron Diffraction Structure Solution of a Nanocrystalline Zeolite at Atomic Resolution. J. Phys. Chem. B**103** (1999) 8245-8250. b) Carlsson, A.; Oku, T.; Bovin, J.-O.; Karlsson, G.; Okamoto, Y.; Ohnishi, N.; Terasaki, O.: The structure of iron oxide implanted zeolite Y, determined by high-resolution electron microscopy and refined with selected area electron diffraction amplitudes. Chem. Eur. J. **5** (1999) 244–249. c) Carlsson, A.; Kaneda, M.; Sakamoto, Y.; Terasaki, O.; Ryoo, R.; Joo, S.H.: The structure of MCM-48 determined by electron crystallography. J. Electron Microsc. **48** (1999) 795–798. d) Ohsuna, T.; Liu, Z.; Terasaki, O.; Hiraga, K.; Camblor, M.A.: Framework determination of a polytype of zeolite Beta by using electron crystallography. J. Phys. Chem. B **106** (2002) 5673-5678.

[26] a) Dorset, D.L.; Roth, W.J.; Gilmore, C.J.: Electron crystallography of zeolites - the MWW family as a test of direct 3D structure determination. Acta Cryst. **A61** (2005) 516–527. b) Dorset, D. L.: The crystal structure of ZSM-10, a powder x-ray and electron diffraction study. Z. Krist. 221 (2006) 260–265. c) Dorset, D. L.; Gilmore, C. J.; Jorda, J. L.; Nicolopoulos, S.: Direct electron crystallographic determination of zeolite zonal structures. Ultramicroscopy **107** (2007) 462-473. d) Gilmore, C. J.; Dong, W.; Dorset, D. L.: Solving the crystal structures of zeolites using electron diffraction. I. Use of potential density histograms. Acta Cryst. **A64** (2008) 284–294. e) Gilmore, C. J.; Dong, W.; Dorset, D. L.: Solving the crystal structures of zeolites using electron diffraction.II. Density building functions. Acta Cryst. **A64** (2008) 295-302. f) Dorset, D. L.; Strohmaier, K. G.; Kliewer, C. E.; Corma, A.; Díaz-Cabanas, M. J.; Rey, F.; Gilmore, C. J.: The crystal structure of ITQ-26, a 3-D framework with extra-large pores. Chem. Mater. **20** (2008) 5325–5331.

[27] Sakamoto, Y.; Kaneda, M. Terasaki, O.; Zhao, D.Y.; Kim, J.M.; Stucky, G.; Shin, H.J.; Ryoo, R.: Direct imaging of the pores and cages of three-dimensional mesoporous materials. Nature **408** (2000) 449–453.

[28] Gao, C.B.; Sakamoto, Y.; Sakamoto, K.; Terasaki, O.; Che, S.A.: Synthesis and characterization of mesoporous silica AMS-10 with bicontinuous cubic Pn-3m symmetry. Angew. Chem. Int. Ed. **45** (2006) 4295–4298.

[29] Ruan, J.F.; Wu, P.; Slater, B.; Terasaki, O. Structure Elucidation of the Highly Active Titanosilicate Catalyst Ti-YNU-1. Angew. Chem. Int. Ed. **44** (2005) 6719–6723.

[30] a) Oszlányi, G.; Süto, A.: *Ab initio* structure solution by charge flipping. Acta Cryst. A**60** (2004) 134–141; b) Oszlányi, G.; Süto, A.: *Ab initio* structure solution by charge flipping. II. Use of weak reflections Acta Cryst. **A61** (2005) 147–152; c) Baerlocher, Ch., McCusker, L.B.; Palatinus, L.: Charge flipping combined with histogram matching to solve complex crystal structures from powder diffraction data. Z. Kristallogr. **222** (2007) 47-53.

[31] Benazzi, E.; Guth, J.L.; Rouleau, L.: Preparation of IM-5 zeolite and its catalytic applications. PCT Int. Appl. WO **98** (1998) 17581.

[32] a) Corma, A.; Chica, A.; Guil, J.M.; Llopis, F.J.; Mabilon, G.; Perdigón-Melón, J.A.; Valencia, S.: Determination of the pore topology of zeolite IM-5 by means of catalytic test reactions and hydrocarbon adsorption measurements. J. Catal. **189** (2000) 382-394; b) Corma, A.; Martínez-Triguero, J.; Valencia, S.; Benazzi, E.; Lacombe, S.: IM-5: A Highly Thermal and Hydrothermal Shape-Selective Cracking Zeolite. J. Catal. **206** (2002) 125–133; c) Lee, S. H.; Lee, D. K.; Shin, C. H.; Park, Y. K.; Wright, P. A.; Lee, W. M.; Hong, S. B.: Synthesis, characterization, and catalytic properties of zeolites IM-5 and NU-88. J. Catal. **215** (2003) 151-170; d) Serra, J. M.; Guillon, E.; Corma,

A.: A rational design of alkyl-aromatics dealkylation-transalkylation catalysts using C_8 and C_9 alkyl-aromatics as reactants. J. Catal. **227** (2004) 459–469.

[33] Zou, X. D.; Sukharev, Yu.; Hovmöller, S.: ELD – A computer program system for extracting intensities from electron diffraction patterns. Ultramicroscopy **49** (1993) 147–158.

[34] Zou, X.D.; Hovmöller, A.; Hovmöller S.: Trice – a program for reconstructing 3D reciprocal space and determining unit cell parameters. Ultramicroscopy **98** (2004) 187–193.

[35] Hovmöller, S.: CRISP – Crystallographic image processing on a personal computer. Ultramicroscopy **41** (1992) 121–135.

[36] Oleynikov, P. http://www.analitex.com.

[37] Baerlocher, Ch.; Hepp, A.; Meier, W.M. DLS-76: Distance-least-squares refinement program. ETH Zürich, Switzerland, 1976.

[38] O'Keefe, M.A.; Dahmen, U.; Hetherington, C.J.D.: Simulated image maps for use in experimental high-resolution electron microscopy. Mat. Res. Soc. Symp. Proc. **159** (1989) 453–458.

[39] Capitani, G.C.; Oleynikov, P.; Hovmöller, S.; Mellini, M. A.: A practical method to detect and correct for lens distortion in the TEM. Ultramicroscopy **106** (2006) 66–74.

[40] Hahn, T. International Tables for Crystallography Vol. A: Space-Group Symmetry. Fifth Edition, Kluwer Academic Publishers (Dordrecht), **2002**.

Supplementary materials

Table S1. The original 281 reflections obtained from HRTEM images along [1 0 0], [0 0 1] and [01 0] directions by the program CRISP.

Table S2. Si positions obtained from the electrostatic map.

Table S3. Final atomic position compared with the position refined by X-ray powder diffraction.

Table S4. CIF of IM-5 after the DLS refinement.

Table S1. The original 281 reflections obtained from HRTEM images along [1 0 0], [0 1 0] and [0 0 1] directions by the program CRISP. $Ampl_{exp}$, $Ampl_{sym}$ and $Ampl_{cal}$ are experimental, symmetry-imposed and calculated (from the model refined by powder XRD data) amplitudes. $Phase_{exp}$, $Phase_{sym}$ and $Phase_{cal}$ are experimental, symmetry-imposed and calculated phases. The CTF correction was done on the phases. (*) Experimental and calculated phases deviate.

From [1 0 0] direction

h	k	l	d-val /Å	$Ampl_{exp}$	$Ampl_{sym}$	$Ampl_{cal}$	$Phase_{exp}$	$Phase_{sym}$	$Phase_{cal}$	
0	0	2	10.00	5113	5112	6184	9	0	0	
0	0	4	5.00	6272	6272	4474	-171	180	180	
0	0	6	3.33	2300	2300	3193	-1	0	0	
0	0	8	2.50	112	112	3662	-49	0	180	*
0	2	1	16.39	206	120	397	-24	0	0	
0	2	-1	16.39	34	120	397	161	180	180	
0	2	2	9.44	396	464	563	14	0	0	
0	2	-2	9.44	532	464	563	8	0	0	
0	2	3	6.49	407	433	158	-40	0	0	
0	2	-3	6.49	459	433	158	161	180	180	
0	2	4	4.92	0	138	111	31	0	180	*
0	2	-4	4.92	275	138	111	-18	0	180	*
0	2	5	3.96	637	504	620	163	180	180	
0	2	-5	3.96	371	504	620	-5	0	0	
0	2	6	3.31	214	107	285	13	0	0	
0	2	-6	3.31	0	107	285	47	0	0	
0	2	7	2.84	94	93	357	171	180	180	
0	2	-7	2.84	92	93	357	-133	0	0	
0	2	8	2.49	65	85	375	-35	0	0	
0	2	-8	2.49	104	85	375	33	0	0	
0	4	0	14.31	101	101	383	-170	180	180	
0	4	1	11.64	3254	3617	4337	11	0	0	

h	k	l	d-val /Å	Ampl$_{exp}$	Ampl$_{sym}$	Ampl$_{cal}$	Phase$_{exp}$	Phase$_{sym}$	Phase$_{cal}$	
0	4	-1	11.64	3981	3617	4337	-175	180	180	
0	4	3	6.04	4531	4893	3351	-164	180	180	
0	4	-3	6.04	5254	4893	3351	5	0	0	
0	4	5	3.85	6804	6832	9587	-172	180	180	
0	4	-5	3.85	6860	6832	9587	3	0	0	
0	4	6	3.25	80	40	201	10	0	180	*
0	4	-6	3.25	0	40	201	-89	0	180	*
0	4	7	2.80	158	104	1508	-57	0	180	*
0	4	-7	2.80	51	104	1508	-158	180	0	*
0	4	9	2.20	49	45	1736	-162	180	0	*
0	4	-9	2.20	40	45	1736	17	0	180	*
0	6	0	9.54	6138	6138	6400	175	180	180	
0	6	1	8.61	472	426	434	24	0	0	
0	6	-1	8.61	381	426	434	180	180	180	
0	6	2	6.90	355	453	625	167	180	180	
0	6	-2	6.90	550	453	625	164	180	180	
0	6	3	5.46	259	369	132	-137	180	180	
0	6	-3	5.46	479	369	132	28	0	0	
0	6	4	4.43	132	143	648	19	0	0	
0	6	-4	4.43	154	143	648	-127	0	0	
0	6	5	3.69	611	569	1126	174	180	180	
0	6	-5	3.69	529	569	1126	17	0	0	
0	6	6	3.15	186	93	1199	163	180	180	
0	6	-6	3.15	0	93	1199	92	180	180	
0	8	0	7.15	3996	3996	3264	0	0	0	
0	8	1	6.74	595	691	540	-13	0	0	
0	8	-1	6.74	785	691	540	163	180	180	
0	8	2	5.82	2159	2524	2196	-174	180	180	
0	8	-2	5.82	2890	2524	2196	-178	180	180	
0	8	3	4.88	437	516	378	151	180	180	
0	8	-3	4.88	594	516	378	-24	0	0	
0	8	4	4.10	187	224	12	102	0	180	*
0	8	-4	4.10	261	224	12	-36	0	180	*
0	8	5	3.49	292	146	642	151	180	180	
0	8	-5	3.49	0	146	642	-28	0	0	
0	8	6	3.02	220	182	809	34	0	0	
0	8	-6	3.02	145	182	809	54	0	0	
0	8	8	2.36	98	76	656	-86	0	180	*
0	8	-8	2.36	54	76	656	-15	0	180	*
0	10	0	5.72	934	934	1294	0	0	0	

h	k	l	d-val /Å	Ampl$_{exp}$	Ampl$_{sym}$	Ampl$_{cal}$	Phase$_{exp}$	Phase$_{sym}$	Phase$_{cal}$	
0	10	1	5.50	416	462	980	179	180	180	
0	10	-1	5.50	508	462	980	-31	0	0	
0	10	2	4.97	361	429	228	-173	180	180	
0	10	-2	4.97	497	429	228	164	180	180	
0	10	3	4.34	950	889	1217	1	0	0	
0	10	-3	4.34	828	889	1217	177	180	180	
0	10	4	3.76	137	108	473	-91	0	180	*
0	10	-4	3.76	78	108	473	-34	0	180	*
0	10	5	3.28	121	257	1771	-36	180	0	*
0	10	-5	3.28	393	257	1771	45	0	180	*
0	10	7	2.56	84	71	832	108	0	180	*
0	10	-7	2.56	60	71	832	145	180	0	*
0	12	0	4.77	1840	1840	1614	170	180	180	
0	12	1	4.64	464	448	823	-53	0	0	
0	12	-1	4.64	431	448	823	143	180	180	
0	12	2	4.30	405	352	404	158	180	180	
0	12	-2	4.30	299	352	404	155	180	180	
0	12	3	3.88	2014	1958	3917	164	180	180	
0	12	-3	3.88	1903	1958	3917	-9	0	0	
0	12	5	3.06	243	186	2389	144	180	180	
0	12	-5	3.06	128	186	2389	-80	0	0	
0	12	6	2.73	0	58	262	107	0	180	*
0	12	-6	2.73	117	58	262	54	0	180	*
0	12	7	2.45	57	164	1369	-95	180	0	*
0	12	-7	2.45	271	164	1369	23	0	180	*
0	14	0	4.09	847	847	1994	178	180	180	
0	14	1	4.01	362	329	688	-31	0	0	
0	14	-1	4.01	298	329	688	143	180	180	
0	14	2	3.78	304	294	352	177	180	180	
0	14	-2	3.78	284	294	352	-173	180	180	
0	14	3	3.48	402	306	1278	153	180	180	
0	14	-3	3.48	209	306	1278	-28	0	0	
0	14	4	3.16	47	86	641	-140	180	0	*
0	14	-4	3.16	125	86	641	-134	180	0	*
0	14	5	2.86	127	203	1600	91	0	180	*
0	14	-5	2.86	279	203	1600	-142	180	0	*
0	14	7	2.34	70	50	977	-158	180	0	*
0	14	-7	2.34	31	50	977	-123	0	180	*
0	16	0	3.58	905	905	3639	-26	0	0	
0	16	1	3.52	154	152	69	157	180	0	*

h	k	l	d-val /Å	Ampl$_{exp}$	Ampl$_{sym}$	Ampl$_{cal}$	Phase$_{exp}$	Phase$_{sym}$	Phase$_{cal}$	
0	16	-1	3.52	152	152	69	-39	0	180	*
0	16	2	3.37	215	210	1456	-20	0	0	
0	16	-2	3.37	204	210	1456	-21	0	0	
0	16	4	2.91	40	47	118	-111	0	180	*
0	16	-4	2.91	54	47	118	39	0	180	*
0	16	5	2.67	29	90	607	-58	180	0	*
0	16	-5	2.67	150	90	607	-3	0	180	*
0	16	6	2.44	47	65	775	176	180	0	*
0	16	-6	2.44	84	65	775	-176	180	0	*
0	16	7	2.23	0	40	764	-85	180	0	*
0	16	-7	2.23	80	40	764	39	0	180	*
0	18	0	3.18	67	67	2181	105	180	180	
0	18	1	3.14	94	47	178	-11	0	180	*
0	18	-1	3.14	0	47	178	-176	180	0	*
0	18	2	3.03	76	60	667	51	0	180	*
0	18	-2	3.03	44	60	667	8	0	180	*
0	18	3	2.87	20	62	207	106	180	180	
0	18	-3	2.87	104	62	207	22	0	0	
0	18	5	2.49	50	71	945	-134	180	0	*
0	18	-5	2.49	92	71	945	62	0	180	*
0	20	1	2.83	140	133	1096	175	180	0	*
0	20	-1	2.83	127	133	1096	3	0	180	*
0	20	3	2.63	100	125	1532	4	0	180	*
0	20	-3	2.63	150	125	1532	-152	180	0	*
0	20	4	2.48	27	45	180	-165	0	0	
0	20	-4	2.48	63	45	180	-56	0	0	
0	20	5	2.33	75	78	2214	-35	0	180	*
0	20	-5	2.33	82	78	2214	-140	180	0	*
0	22	1	2.58	86	75	359	87	180	180	
0	22	-1	2.58	63	75	359	22	0	0	
0	24	0	2.38	70	70	1614	-65	0	180	*

From [0 0 1] direction

h	k	l	d-val /Å	Ampl$_{exp}$	Ampl$_{sym}$	Ampl$_{cal}$	Phase$_{exp}$	Phase$_{sym}$	Phase$_{cal}$	
0	6	0	9.54	5565	5565	6400	156	180	180	
0	8	0	7.15	1827	1827	3264	-18	0	0	
0	10	0	5.72	1341	1341	1294	-12	0	0	
0	12	0	4.77	2198	2198	1614	159	180	180	
0	14	0	4.09	1577	1577	1994	-178	180	180	
0	16	0	3.58	1587	1587	3639	24	0	0	
0	18	0	3.18	631	631	2181	-173	180	180	
0	26	0	2.20	244	244	991	-176	180	0	*

h	k	l	d-val /Å	Ampl$_{exp}$	Ampl$_{sym}$	Ampl$_{cal}$	Phase$_{exp}$	Phase$_{sym}$	Phase$_{cal}$	
0	30	0	1.91	117	117	2208	-175	180	0	*
1	3	0	11.40	3236	4185	5342	155	180	180	
1	-3	0	11.40	5134	4185	5342	-176	180	180	
1	5	0	8.91	246	305	28	-147	180	180	
1	-5	0	8.91	364	305	28	102	180	180	
1	7	0	7.09	2065	2097	2170	169	180	180	
1	-7	0	7.09	2128	2097	2170	173	180	180	
1	9	0	5.80	728	1401	550	172	180	180	
1	-9	0	5.80	2076	1401	550	-170	180	180	
1	11	0	4.89	247	430	107	154	180	180	
1	-11	0	4.89	613	430	107	-147	180	180	
1	13	0	4.21	0	423	674	43	0	0	
1	-13	0	4.21	846	423	674	-11	0	0	
1	15	0	3.69	2377	3950	5153	3	0	0	
1	-15	0	3.69	5521	3950	5153	-13	0	0	
1	17	0	3.28	172	133	234	108	0	0	
1	-17	0	3.28	93	133	234	-50	0	0	
1	19	0	2.95	100	133	1066	93	0	180	*
1	-19	0	2.95	167	133	1066	-72	0	180	*
1	21	0	2.68	111	179	744	30	0	180	*
1	-21	0	2.68	247	179	744	85	0	180	*
2	0	0	7.10	7483	7483	5481	178	180	180	
2	2	0	6.90	0	340	105	-58	180	0	*
2	-2	0	6.90	681	340	105	170	180	0	*
2	6	0	5.70	3219	6131	3973	-179	180	180	
2	-6	0	5.70	9042	6131	3973	-178	180	180	
2	8	0	5.04	840	1528	1534	171	180	180	
2	-8	0	5.04	2217	1528	1534	171	180	180	
2	10	0	4.46	513	1006	983	-14	0	0	
2	-10	0	4.46	1498	1006	983	-8	0	0	
2	12	0	3.96	311	156	388	52	0	0	
2	-12	0	3.96	0	156	388	-61	0	0	
2	14	0	3.54	0	615	1187	-138	180	180	
2	-14	0	3.54	1228	615	1187	178	180	180	
2	16	0	3.20	199	425	3565	-44	180	180	
2	-16	0	3.20	652	425	3565	127	180	180	
2	20	0	2.65	126	192	1285	-168	180	0	*
2	-20	0	2.65	260	192	1285	162	180	0	*
3	1	0	4.72	0	283	37	-176	180	0	*
3	-1	0	4.72	566	283	37	172	180	0	*

h	k	l	d-val /Å	Ampl$_{exp}$	Ampl$_{sym}$	Ampl$_{cal}$	Phase$_{exp}$	Phase$_{sym}$	Phase$_{cal}$	
3	3	0	4.60	948	1301	1281	12	0	0	
3	-3	0	4.60	1654	1301	1281	15	0	0	
3	5	0	4.38	0	326	638	-69	0	0	
3	-5	0	4.38	650	326	638	50	0	0	
3	9	0	3.80	2493	6803	8490	11	0	0	
3	-9	0	3.80	11113	6803	8490	0	0	0	
3	13	0	3.22	0	434	2058	43	0	0	
3	-13	0	3.22	868	434	2058	-28	0	0	
3	17	0	2.74	246	179	1227	-29	0	0	
3	-17	0	2.74	111	179	1227	155	0	0	
3	21	0	2.36	0	401	2310	97	0	180	*
3	-21	0	2.36	801	401	2310	-31	0	180	*
3	23	0	2.20	137	124	1236	126	180	180	
3	-23	0	2.20	111	124	1236	-46	180	180	
3	25	0	2.06	110	268	1722	1	180	0	*
3	-25	0	2.06	425	268	1722	105	180	0	*
4	0	0	3.55	4278	4278	10000	17	0	0	
4	2	0	3.53	399	335	458	167	180	180	
4	-2	0	3.53	271	335	458	150	180	180	
4	4	0	3.45	254	299	802	-174	180	180	
4	-4	0	3.45	344	299	802	-78	180	180	
4	6	0	3.33	695	1093	4512	-177	180	180	
4	-6	0	3.33	1490	1093	4512	160	180	180	
4	10	0	3.02	0	256	266	-161	0	0	
4	-10	0	3.02	512	256	266	-14	0	0	
4	12	0	2.85	95	244	137	-37	0	0	
4	-12	0	2.85	392	244	137	-32	0	0	
4	14	0	2.68	230	254	606	-124	0	180	*
4	-14	0	2.68	280	254	606	15	0	180	*
4	18	0	2.37	29	187	264	-166	0	0	
4	-18	0	2.37	344	187	264	23	0	0	
4	20	0	2.23	199	188	238	72	180	0	*
4	-20	0	2.23	178	188	238	122	180	0	*
4	24	0	1.98	95	346	3405	76	180	0	*
4	-24	0	1.98	595	346	3405	134	180	0	*
5	3	0	2.81	276	378	3070	-57	0	180	*
5	-3	0	2.81	479	378	3070	-46	0	180	*
5	7	0	2.68	0	127	1125	-52	180	180	
5	-7	0	2.68	254	127	1125	-144	180	180	
5	9	0	2.59	0	530	1877	-75	0	180	*

h	k	l	d-val /Å	Ampl$_{exp}$	Ampl$_{sym}$	Ampl$_{cal}$	Phase$_{exp}$	Phase$_{sym}$	Phase$_{cal}$	
5	-9	0	2.59	1061	530	1877	-13	0	180	*
5	11	0	2.49	206	222	1162	-121	0	180	*
5	-11	0	2.49	239	222	1162	30	0	180	*
5	15	0	2.28	0	160	678	-49	180	0	*
5	-15	0	2.28	321	160	678	125	180	0	*
5	31	0	1.55	156	133	639	-71	180	0	*
5	-31	0	1.55	111	133	639	-143	180	0	*
5	33	0	1.48	68	122	965	-155	180	0	*
5	-33	0	1.48	177	122	965	117	180	0	*
6	0	0	2.37	226	226	1107	148	180	0	*
6	4	0	2.34	0	118	728	133	180	0	*
6	-4	0	2.34	235	118	728	175	180	0	*
6	8	0	2.25	86	129	620	-167	0	180	*
6	-8	0	2.25	171	129	620	43	0	180	*
6	18	0	1.90	102	189	455	119	180	0	*
6	-18	0	1.90	276	189	455	-167	180	0	*
7	7	0	1.97	131	154	683	-105	0	180	*
7	-7	0	1.97	174	154	683	-59	0	180	*
7	9	0	1.93	0	189	5487	-130	180	0	*
7	-9	0	1.93	378	189	5487	150	180	0	*
7	15	0	1.79	69	124	3197	24	0	180	*
7	-15	0	1.79	181	124	3197	20	0	180	*
9	5	0	1.56	154	118	112	88	0	0	
9	-5	0	1.56	84	118	112	11	0	0	
10	8	0	1.39	152	128	619	111	180	0	*
10	-8	0	1.39	104	128	619	-174	180	0	*

From [0 1 0] direction

h	k	l	d-val /Å	Ampl$_{exp}$	Ampl$_{sym}$	Ampl$_{cal}$	Phase$_{exp}$	Phase$_{sym}$	Phase$_{cal}$	
0	0	2	10.00	4231	4231	6184	7	0	0	
0	0	4	5.00	5289	5289	4474	180	180	180	
0	0	6	3.33	4165	4165	3193	-1	0	0	
0	0	8	2.50	997	997	3662	178	180	180	
0	0	10	2.00	1274	1274	8153	-159	180	180	
2	0	0	7.10	5556	5556	5481	133	180	180	
2	0	2	5.79	1429	865	964	125	180	180	
2	0	-2	5.79	300	865	964	119	180	180	
2	0	6	3.02	259	130	239	-35	0	180	*
2	0	-6	3.02	0	130	239	-132	0	180	*
2	0	8	2.36	376	294	26	119	180	180	
2	0	-8	2.36	212	294	26	112	180	180	
2	0	10	1.92	479	311	1068	165	180	0	*

h	k	l	d-val /Å	Ampl$_{exp}$	Ampl$_{sym}$	Ampl$_{cal}$	Phase$_{exp}$	Phase$_{sym}$	Phase$_{cal}$	
2	0	-10	1.92	145	311	1068	24	180	0	*
4	0	0	3.55	15722	15722	10000	0	0	0	
4	0	2	3.35	2223	1871	1637	-3	0	0	
4	0	-2	3.35	1519	1871	1637	-2	0	0	
4	0	4	2.90	1338	811	916	159	180	180	
4	0	-4	2.90	285	811	916	-156	180	180	
4	0	6	2.43	616	440	784	-50	0	0	
4	0	-6	2.43	265	440	784	134	0	0	
4	0	8	2.04	242	258	364	26	0	0	
4	0	-8	2.04	275	258	364	7	0	0	
4	0	10	1.74	241	233	1856	23	0	180	*
4	0	-10	1.74	226	233	1856	-44	0	180	*
6	0	0	2.37	1179	1179	1107	14	0	0	
6	0	2	2.30	436	335	396	-1	0	0	
6	0	-2	2.30	233	335	396	15	0	0	
6	0	4	2.14	280	156	1025	29	0	0	
6	0	-4	2.14	32	156	1025	98	0	0	
8	0	0	1.78	479	479	925	176	180	0	*
8	0	2	1.75	157	139	196	-167	180	0	*
8	0	-2	1.75	119	139	196	178	180	0	*
10	0	0	1.42	139	139	5962	-164	180	0	*

Table S2. Si positions obtained from the electrostatic map.

Atoms	x	y	z
Si1	0.00	0.070	0.05
Si2	0.00	0.123	0.16
Si3	0.00	0.209	0.16
Si4	0.00	0.261	0.06
Si5	0.00	0.406	0.16
Si6	0.00	0.464	0.15
Si7	0.20	0.065	0.05
Si8	0.20	0.137	0.16
Si9	0.20	0.186	0.14
Si10	0.20	0.271	0.05
Si11	0.20	0.392	0.15
Si12	0.20	0.490	0.16
Si13	0.30	0.019	0.05
Si14	0.30	0.110	0.05
Si15	0.30	0.231	0.16
Si16	0.30	0.318	0.05
Si17	0.30	0.359	0.06
Si18	0.30	0.437	0.15
Si19	0.50	0.042	0.05
Si20	0.50	0.098	0.06
Si21	0.50	0.249	0.16
Si22	0.50	0.286	0.05
Si23	0.50	0.388	0.05
Si24	0.50	0.424	0.15

Table S3. Final atomic position compared with the position refined by X-ray powder diffraction.

Atoms	x_{HRTEM}	x_{xray}	y_{HRTEM}	y_{xray}	z_{HRTEM}	z_{xray}	$\delta_x/Å$	$\delta_y/Å$	$\delta_z/Å$	$\delta/Å$
Si1	0.000	0.0000	0.0818(9)	0.0819	0.058(2)	0.0561	0.000	0.004	0.039	0.039
Si2	0.000	0.0000	0.1188(12)	0.1132	0.176(2)	0.1733	0.000	0.322	0.060	0.328
Si3	0.000	0.0000	0.2083(11)	0.2106	0.174(2)	0.1727	0.000	0.133	0.019	0.135
Si4	0.000	0.0000	0.2454(8)	0.2465	0.058(2)	0.0596	0.000	0.061	0.034	0.070
Si5	0.000	0.0000	0.3991(9)	0.4051	0.126(3)	0.1313	0.000	0.343	0.105	0.358
Si6	0.000	0.0000	0.4558(8)	0.4575	0.125(3)	0.1235	0.000	0.097	0.034	0.103
Si7	0.196(2)	0.1985	0.0605(6)	0.0628	0.030(2)	0.0304	0.034	0.129	0.010	0.134
Si8	0.203(2)	0.1956	0.1379(7)	0.1369	0.173(1)	0.1699	0.107	0.058	0.070	0.140
Si9	0.195(2)	0.1866	0.1895(7)	0.1887	0.129(2)	0.1224	0.123	0.047	0.136	0.188
Si10	0.203(1)	0.2028	0.2639(4)	0.2642	0.060(1)	0.0611	0.005	0.017	0.012	0.022
Si11	0.203(1)	0.2029	0.3911(8)	0.3906	0.174(1)	0.1738	0.007	0.030	0.003	0.031
Si12	0.187(2)	0.1893	0.4801(6)	0.4811	0.173(1)	0.1712	0.032	0.059	0.042	0.079
Si13	0.318(3)	0.3125	0.0180(3)	0.0179	0.061(1)	0.0611	0.083	0.003	0.008	0.084
Si14	0.295(1)	0.2938	0.1069(3)	0.1083	0.064(2)	0.0677	0.014	0.081	0.072	0.109
Si15	0.299(2)	0.2941	0.2350(8)	0.2331	0.173(1)	0.1711	0.073	0.110	0.043	0.139
Si16	0.304(2)	0.3075	0.3106(5)	0.3105	0.028(2)	0.0371	0.048	0.005	0.188	0.193
Si17	0.295(1)	0.2964	0.3637(5)	0.3621	0.055(2)	0.0538	0.025	0.094	0.032	0.102
Si18	0.305(2)	0.3042	0.4374(8)	0.4364	0.128(2)	0.1298	0.006	0.060	0.035	0.069
Si19	0.500	0.5000	0.0444(7)	0.0430	0.025(3)	0.0369	0.000	0.080	0.234	0.246

Si20	0.500	0.5000	0.1009(8)	0.0954	0.025(3)	0.0294	0.000	0.316	0.089	0.328
Si21	0.500	0.5000	0.2528(12)	0.2532	0.172(2)	0.1767	0.000	0.026	0.099	0.102
Si22	0.500	0.5000	0.2913(8)	0.2905	0.063(2)	0.0600	0.000	0.048	0.053	0.071
Si23	0.500	0.5000	0.3810(9)	0.3796	0.061(2)	0.0567	0.000	0.081	0.079	0.113
Si24	0.500	0.5000	0.4173(11)	0.4182	0.173(1)	0.1718	0.000	0.051	0.019	0.054
O1	0.092(1)	0.0899	0.0655(9)	0.0656	0.058(4)	0.0485	0.036	0.003	0.182	0.184
O2	0.000	0.0000	0.0986(13)	0.1049	-0.006(3)	0.0101	0.000	0.362	0.320	0.482
O3	0.000	0.0000	0.0976(15)	0.0891	0.124(3)	0.1333	0.000	0.489	0.189	0.524
O4	0.092(1)	0.0901	0.1349(12)	0.1285	0.166(5)	0.1544	0.022	0.366	0.236	0.436
O5	0.000	0.0000	0.1081(24)	0.1052	0.250	0.2500	0.000	0.165	0.000	0.165
O6	0.000	0.0000	0.2168(21)	0.2177	0.250	0.2500	0.000	0.052	0.000	0.052
O7	0.092(1)	0.0887	0.1927(11)	0.1947	0.160(3)	0.1571	0.052	0.113	0.063	0.139
O8	0.000	0.0000	0.2311(12)	0.2348	0.126(3)	0.1327	0.000	0.214	0.126	0.248
O9	0.000	0.0000	0.2274(10)	0.2255	-0.003(3)	0.0061	0.000	0.108	0.185	0.213
O10	0.091(1)	0.0907	0.2622(7)	0.2628	0.054(2)	0.0525	0.003	0.034	0.039	0.052
O11	0.000	0.0000	0.4275(8)	0.4318	0.128(6)	0.1541	0.000	0.249	0.529	0.582
O12	0.092(1)	0.0917	0.3890(10)	0.3920	0.163(3)	0.1591	0.004	0.171	0.069	0.184
O13	0.000	0.0000	0.3900(18)	0.4055	0.050(3)	0.0510	0.000	0.888	0.010	0.888
O14	0.000	0.0000	0.4650(15)	0.4589	0.050(3)	0.0433	0.000	0.346	0.129	0.369
O15	0.091(1)	0.0887	0.4660(11)	0.4708	0.162(3)	0.1528	0.031	0.277	0.194	0.339
O16	0.226(2)	0.2321	0.0341(7)	0.0371	0.050(3)	0.0500	0.078	0.171	0.007	0.188

O17	0.197(5)	0.2071	0.0632(12)	0.0668	-0.049(2)	-0.0495	0.139	0.205	0.012	0.248
O18	0.269(2)	0.2600	0.0792(7)	0.0815	0.061(3)	0.0705	0.128	0.133	0.186	0.261
O19	0.233(3)	0.2168	0.1633(7)	0.1623	0.145(4)	0.1388	0.232	0.057	0.115	0.265
O20	0.256(3)	0.2687	0.1175(9)	0.1177	0.132(2)	0.1417	0.186	0.010	0.186	0.263
O21	0.232(7)	0.2075	0.1362(16)	0.1379	0.250	0.2500	0.351	0.094	0.000	0.364
O22	0.266(3)	0.2641	0.2082(9)	0.2072	0.162(3)	0.1478	0.032	0.058	0.282	0.288
O23	0.191(5)	0.1763	0.1934(13)	0.1915	0.051(2)	0.0425	0.209	0.108	0.165	0.287
O24	0.235(2)	0.2365	0.2912(4)	0.2910	0.059(2)	0.0642	0.023	0.010	0.098	0.100
O25	0.250	0.2500	0.250	0.2500	0.000	0.0000	0.000	0.000	0.000	0.000
O26	0.236(3)	0.2319	0.2524(9)	0.2522	0.129(1)	0.1311	0.051	0.009	0.035	0.062
O27	0.227(4)	0.2197	0.3852(17)	0.3815	0.250	0.2500	0.105	0.212	0.000	0.237
O28	0.257(3)	0.2561	0.3729(10)	0.3735	0.126(2)	0.1220	0.015	0.034	0.078	0.086
O29	0.235(3)	0.2413	0.4177(9)	0.4168	0.158(4)	0.1651	0.085	0.054	0.153	0.182
O30	0.273(2)	0.2654	0.4632(8)	0.4616	0.153(3)	0.1514	0.112	0.094	0.036	0.150
O31	0.189(5)	0.2096	0.5036(6)	0.5046	0.129(1)	0.1301	0.286	0.060	0.026	0.293
O32	0.197(5)	0.1924	0.4873(11)	0.4877	0.250	0.2500	0.063	0.022	0.000	0.067
O33	0.409(1)	0.4100	0.0349(10)	0.0313	0.064(3)	0.0703	0.017	0.207	0.136	0.248
O34	0.329(7)	0.3219	0.000	0.0000	0.000	0.0000	0.096	0.000	0.000	0.096
O35	0.407(1)	0.4061	0.1102(8)	0.1083	0.062(3)	0.0554	0.011	0.108	0.125	0.165
O36	0.248(4)	0.2429	0.1202(10)	0.1247	0.003(2)	0.0124	0.072	0.256	0.197	0.330
O37	0.408(1)	0.4064	0.2379(11)	0.2379	0.153(3)	0.1635	0.017	0.002	0.219	0.219

O38	0.287(5)	0.2689	0.2418(13)	0.2358	0.250	0.2500	0.261	0.345	0.000	0.432
O39	0.407(1)	0.4094	0.3076(7)	0.3067	0.059(3)	0.0685	0.027	0.049	0.200	0.207
O40	0.265(3)	0.2642	0.3366(5)	0.3353	0.044(4)	0.0563	0.005	0.073	0.244	0.254
O41	0.407(1)	0.4095	0.3651(9)	0.3629	0.053(3)	0.0559	0.031	0.125	0.055	0.140
O42	0.409(1)	0.4112	0.4325(10)	0.4339	0.154(3)	0.1537	0.028	0.079	0.002	0.084
O43	0.500	0.5000	0.0726(6)	0.0697	0.025(6)	0.0606	0.000	0.167	0.719	0.734
O44	0.500	0.5000	0.2579(24)	0.2647	0.250	0.2500	0.000	0.389	0.000	0.389
O45	0.500	0.5000	0.2774(12)	0.2749	0.132(3)	0.1262	0.000	0.142	0.119	0.185
O46	0.500	0.5000	0.3928(12)	0.3956	0.133(2)	0.1232	0.000	0.159	0.197	0.252
O47	0.500	0.5000	0.4115(20)	0.4107	0.250	0.2500	0.000	0.048	0.000	0.048

Table S4. CIF of IM-5 after the DLS refinement.

data_IM-5fromHRTEM
_audit_creation_method   'generated by CrystalMaker 7.1.7'
_cell_length_a   14.33(4)
_cell_length_b   56.9(2)
_cell_length_c   20.32(7)
_cell_angle_alpha   90.0000
_cell_angle_beta   90.0000
_cell_angle_gamma   90.0000

_symmetry_space_group_name_H-M   'C 2/m 2/c 21/m'
_symmetry_Int_Tables_number   63
_symmetry_cell_setting   orthorhombic
loop_
_symmetry_equiv_pos_as_xyz
'+x,+y,+z'
'1/2+x,1/2+y,+z'
'-x,+y,+z'
'1/2-x,1/2+y,+z'
'+x,-y,1/2+z'
'1/2+x,1/2-y,1/2+z'
'-x,-y,1/2+z'
'1/2-x,1/2-y,1/2+z'
'-x,-y,-z'
'1/2-x,1/2-y,-z'
'+x,-y,-z'
'1/2+x,1/2-y,-z'
'-x,+y,1/2-z'
'1/2-x,1/2+y,1/2-z'
'+x,+y,1/2-z'
'1/2+x,1/2+y,1/2-z'

loop_
_atom_site_type_symbol
_atom_site_label
_atom_site_fract_x
_atom_site_fract_y
_atom_site_fract_z
    Si   Si1   0.000   0.0818(9)   0.058(2)
    Si   Si2   0.000   0.1188(12)   0.176(2)
    Si   Si3   0.000   0.2083(11)   0.174(2)
    Si   Si4   0.000   0.2454(8)   0.058(2)
    Si   Si5   0.000   0.3991(9)   0.126(3)

Si	Si6	0.000	0.4558(8)	0.125(3)
Si	Si7	0.196(2)	0.0605(6)	0.030(2)
Si	Si8	0.203(2)	0.1379(7)	0.173(1)
Si	Si9	0.195(2)	0.1895(7)	0.129(2)
Si	Si10	0.203(1)	0.2639(4)	0.060(1)
Si	Si11	0.203(1)	0.3911(8)	0.174(1)
Si	Si12	0.187(2)	0.4801(6)	0.173(1)
Si	Si13	0.318(3)	0.0180(3)	0.061(1)
Si	Si14	0.295(1)	0.1069(3)	0.064(2)
Si	Si15	0.299(2)	0.2350(8)	0.173(1)
Si	Si16	0.304(2)	0.3106(5)	0.028(2)
Si	Si17	0.295(1)	0.3637(5)	0.055(2)
Si	Si18	0.305(2)	0.4374(8)	0.128(2)
Si	Si19	0.500	0.0444(7)	0.025(3)
Si	Si20	0.500	0.1009(8)	0.025(3)
Si	Si21	0.500	0.2528(12)	0.172(2)
Si	Si22	0.500	0.2913(8)	0.063(2)
Si	Si23	0.500	0.3810(9)	0.061(2)
Si	Si24	0.500	0.4173(11)	0.173(1)
O	O1	0.092(1)	0.0655(9)	0.058(4)
O	O2	0.000	0.0986(13)	-0.006(3)
O	O3	0.000	0.0976(15)	0.124(3)
O	O4	0.092(1)	0.1349(12)	0.166(5)
O	O5	0.000	0.1081(24)	0.250
O	O6	0.000	0.2168(21)	0.250
O	O7	0.092(1)	0.1927(11)	0.160(3)
O	O8	0.000	0.2311(12)	0.126(3)
O	O9	0.000	0.2274(10)	-0.003(3)
O	O10	0.091(1)	0.2622(7)	0.054(2)
O	O11	0.000	0.4275(8)	0.128(6)
O	O12	0.092(1)	0.3890(10)	0.163(3)
O	O13	0.000	0.3900(18)	0.050(3)
O	O14	0.000	0.4650(15)	0.050(3)
O	O15	0.091(1)	0.4660(11)	0.162(3)
O	O16	0.226(2)	0.0341(7)	0.050(3)
O	O17	0.197(5)	0.0632(12)	-0.049(2)
O	O18	0.269(2)	0.0792(7)	0.061(3)
O	O19	0.233(3)	0.1633(7)	0.145(4)
O	O20	0.256(3)	0.1175(9)	0.132(2)
O	O21	0.232(7)	0.1362(16)	0.250
O	O22	0.266(3)	0.2082(9)	0.162(3)
O	O23	0.191(5)	0.1934(13)	0.051(2)
O	O24	0.235(2)	0.2912(4)	0.059(2)
O	O25	0.250	0.250	0.000

O	O26	0.236(3)	0.2524(9)	0.129(1)
O	O27	0.227(4)	0.3852(17)	0.250
O	O28	0.257(3)	0.3729(10)	0.126(2)
O	O29	0.235(3)	0.4177(9)	0.158(4)
O	O30	0.273(2)	0.4632(8)	0.153(3)
O	O31	0.189(5)	0.5036(6)	0.129(1)
O	O32	0.197(5)	0.4873(11)	0.250
O	O33	0.409(1)	0.0349(10)	0.064(3)
O	O34	0.329(7)	0.000	0.000
O	O35	0.407(1)	0.1102(8)	0.062(3)
O	O36	0.248(4)	0.1202(10)	0.003(2)
O	O37	0.408(1)	0.2379(11)	0.153(3)
O	O38	0.287(5)	0.2418(13)	0.250
O	O39	0.407(1)	0.3076(7)	0.059(3)
O	O40	0.265(3)	0.3366(5)	0.044(4)
O	O41	0.407(1)	0.3651(9)	0.053(3)
O	O42	0.409(1)	0.4325(10)	0.154(3)
O	O43	0.500	0.0726(6)	0.025(6)
O	O44	0.500	0.2579(24)	0.250
O	O45	0.500	0.2774(12)	0.132(3)
O	O46	0.500	0.3928(12)	0.133(2)
O	O47	0.500	0.4115(20)	0.250